Practical Radiation Oncology® (2026) 000, e1−e12

practical radiation oncology pro
www.practicalradonc.org

Basic Original Report

Three-Step Image Guidance Strategy for Rectal Anterior Wall Margin Reduction in Hypofractionated Prostate Radiation Therapy

Yan Gao, MM,[a] Lei Huang, MS,[a] Bo Zhao, PhD,[b] Lin Ma, MD,[a] Xuesong Li, MD,[c] Ximeng Deng, MM,[a] Mingwei Ma, MD,[a] Xueying Ren, MD,[a] Jiayan Chen, MD,[a] Hongzhen Li, MD,[a] and Xianshu Gao, MD, PhD[a,*]

[a]Department of Radiotherapy, Peking University First Hospital, Beijing, China; [b]Department of Accelerator and Medical Physics, Institute for Quantum Medical Science, National Institutes for Quantum Science and Technology (QST), Chiba, Japan; and [c]Department of Urology, Peking University First Hospital, Beijing, China

Received 28 May 2025; accepted 22 October 2025

Purpose: This study evaluates a 3-step image guidance strategy (bone-prostate-rectal anterior wall alignment) to reduce posterior clinical target volume-planning target volume (CTV-PTV) margins in hypofractionated prostate radiation therapy while preserving target coverage and minimizing rectal toxicity.

Methods and Materials: Twenty-three patients (575 daily cone beam computed tomography scans) underwent a 3-step alignment protocol: bony alignment, prostate soft-tissue matching, and rectal anterior wall fine-tuning. A dose calculation and hybrid deformable image registration-based workflow was created to accumulate the delivered dose. A 5-mm CTV-PTV margin (0 mm posteriorly) with 70 Gy/25 fractions and strict rectal constraints was used. The deformable image registration uncertainty has been thoroughly evaluated, covering geometric indicators, deformation vector field physical properties, spatial uncertainty, and dosimetric uncertainty indicators. Normal tissue complication probability for grade ≥2 gastrointestinal (GI) and genitourinary (GU) toxicity was calculated using the Lyman-Kutcher-Burman model. Statistical comparisons employed paired t-tests or Wilcoxon rank tests ($P < .05$).

Results: The dice similarity coefficient for CTV, rectum, and bladder exceeded 0.8, with mean distance to agreement under 3 mm. Jacobian determinant analysis showed biomechanical validity, with most voxels deforming within physiological ranges (92.23% for CTV, 89.63% for rectum, and 88.96% for bladder) and no nonphysical deformations. The distance discordance metric varied from 0.01 mm to 10.25 mm, and the δ index showed a 90.04% average passing rate within the PD80%. Compared to prostate-only alignment, rectal normal tissue complication probability was significantly reduced with the 3-step strategy (7.95% vs 13.61%, $P < .01$), with comparable CTV coverage (D95%:69.98 Gy delivered vs 70.98 Gy planned, $P = .08$). Deformable dose accumulation confirmed adequate dominant intraprostatic lesion (DIL) coverage (median D100 %: 71.51 Gy), except for DILs <0.7 mm from the rectal wall, or the rectal volume overlapping with $DIL_{2\ cm}$ (DIL extends uniformly outward by 2 cm) >1.5 cm^3 (requiring 2-3 mm margin expansion).

Conclusions: A 3-step image guidance protocol enhanced rectal protection while maintaining target coverage compared to prostate-only alignment. Reducing the posterior PTV margin preserved CTV coverage, but DIL coverage varied by location. If the DIL is less than 0.7 mm from the rectum or overlaps more than 1.5 cm^3 within 2 mm of the rectum, the reduced margin may not be suitable, potentially

Sources of support: National High-level Hospital Clinical Research Funding (Scientific Research Seed Fund of Peking University First Hospital) (2023SF04).

Research data are stored in an institutional repository and will be shared on request to the corresponding author.

*Corresponding author: Gao Xianshu, MD, PhD; Email: doctorgaoxs@126.com

https://doi.org/10.1016/j.prro.2025.10.020

compromising DIL coverage, suggesting the need for personalized margins and adaptive radiation therapy to prevent underdosage.

Introduction

Radiation therapy for prostate cancer faces a critical challenge in balancing tumor control and organ-at-risk (OAR) protection. Although hypofractionated regimens improve therapeutic efficiency, interfractional pelvic organ motion and deformation often lead to discrepancies between planned and delivered doses, increasing risks of rectal toxicity and target underdosing.[1-3] Current protocols utilize clinical target volume-planning target volume (CTV-PTV) margins to account for positional uncertainties,[4-6] with reduced posterior margins (<5 mm) shown to lower rectal toxicity (grade ≥2 incidence: 10.7%-23.8% over 5 years).[7-10] Some units use a 0 mm margin to protect the rectum, as seen in the conventional versus hypofractionated high-dose intensity-modulated radiotherapy for prostate cancer (CHHiP) study, which implemented complete rectal revision and demonstrated that a reduced margin has a lowered rectal and bladder toxicity (>grade I).[11] However, margin reduction risks inadequate coverage of CTV, especially dominant intraprostatic lesions (DILs), which are primarily responsible for disease recurrence.[12-14] Insufficient targeting of DIL is an independent risk factor for biochemical failure.[15] This paradox underscores the need for precision image guidance to reconcile rectal sparing and target coverage.

Existing strategies, such as prostate-only cone beam computed tomography (CBCT) alignment or fiducial-based matching, inadequately address anterior rectal wall variability —a key determinant of GI toxicity.[16-18] Moreover, conventional deformable image registration (DIR) struggles with bladder/rectal volume changes and interobserver variability,[19-21] limiting its utility in dose accumulation. To address these challenges, we suggest a 3-step image guidance protocol: (1) initial bone alignment, (2) prostate soft-tissue alignment, and (3) fine-tuning of the anterior rectal wall. This approach, paired with a calculation-based and hybrid DIR-based dose accumulation process, adjusts to daily anatomical variations and measures cumulative OAR doses.

This study pioneers the application of daily iterative CBCT (iCBCT) and hybrid DIR to validate the safety of posterior margin elimination (0 mm) in hypofractionated prostate radiation therapy. By correlating delivered dose with biological indices, like equivalent uniform dose (EUD) and normal tissue complication probability (NTCP), we aim to establish a framework for optimizing therapeutic ratios in hypofractionated regimens. Additionally, this research aims to provide a reference for treatment strategies and image guidance in prostate hypofractionated radiation therapy.

Methods and Materials

Patients and iCBCT image preparation

Under exempt approval from the Institutional Review Board, we enrolled 23 patients with prostate cancer undergoing radical radiation therapy between April 2022 and March 2023. The prescription and delineation of radiation therapy dose volumes are guided by the recommendations set forth by the International Commission on Radiation Units and Measurements.[22] DILs are the tumor lesions visible on prostate-specific membrane antigen (PSMA) positron emission tomography (PET)/computed tomography (CT) (PSMA-PET/CT) and multiparametric magnetic resonance imaging (mpMRI). The urethra was delineated in all patients utilizing the sagittal and axial images obtained from the thin-section 3-dimensional T2-weighted turbo spin echo sequence. CTV was defined as the entire prostate and part of the seminal vesicles. PTV was generated by adding 5 mm margins to CTV in all directions except for 0 mm margin to the anterior rectal wall without loss of DILs and given 70 Gy in 25 fractions (70 Gy/2.8 Gy/25 f).

The target adjacent to the rectum's anterior wall requires a dose of 65 Gy, as illustrated in Figure E1. The dosimetric objective was to cover 98% of the CTV with the 95% prescription isodose line and 100% of the DILs with the 95% prescription isodose line.

The volumetric modulated arc therapy plans were created using the Eclipse system (v15.6, Varian) with a 2.5-mm-dose grid, and adopt the analytical anisotropic algorithm . Treatment was conducted on the Halcyon (v3.0, Varian) in FFF mode at 800 MU/min. Patients followed a rectum emptying and bladder filling protocol. The structure generated by the 65 Gy dose-line (Dose_65Gy) served as a reference for daily iCBCT (Fig. 2). Some images were excluded due to unacceptable artifacts and excessive rectal gas. A total of 575 iCBCT image sets were acquired. Subsequently, the CT-simulation and iCBCT images, along with planning doses, structures, and couch shift values, were sent to MIM (MIMVista v7.1.6, MIM Software Inc.) for dose accumulation.

Dose accumulation workflow

An automated contour propagation and dose accumulation workflow using DIR and daily calculated dose in synthetic CT (sCT) was developed, as shown in Figure 1.

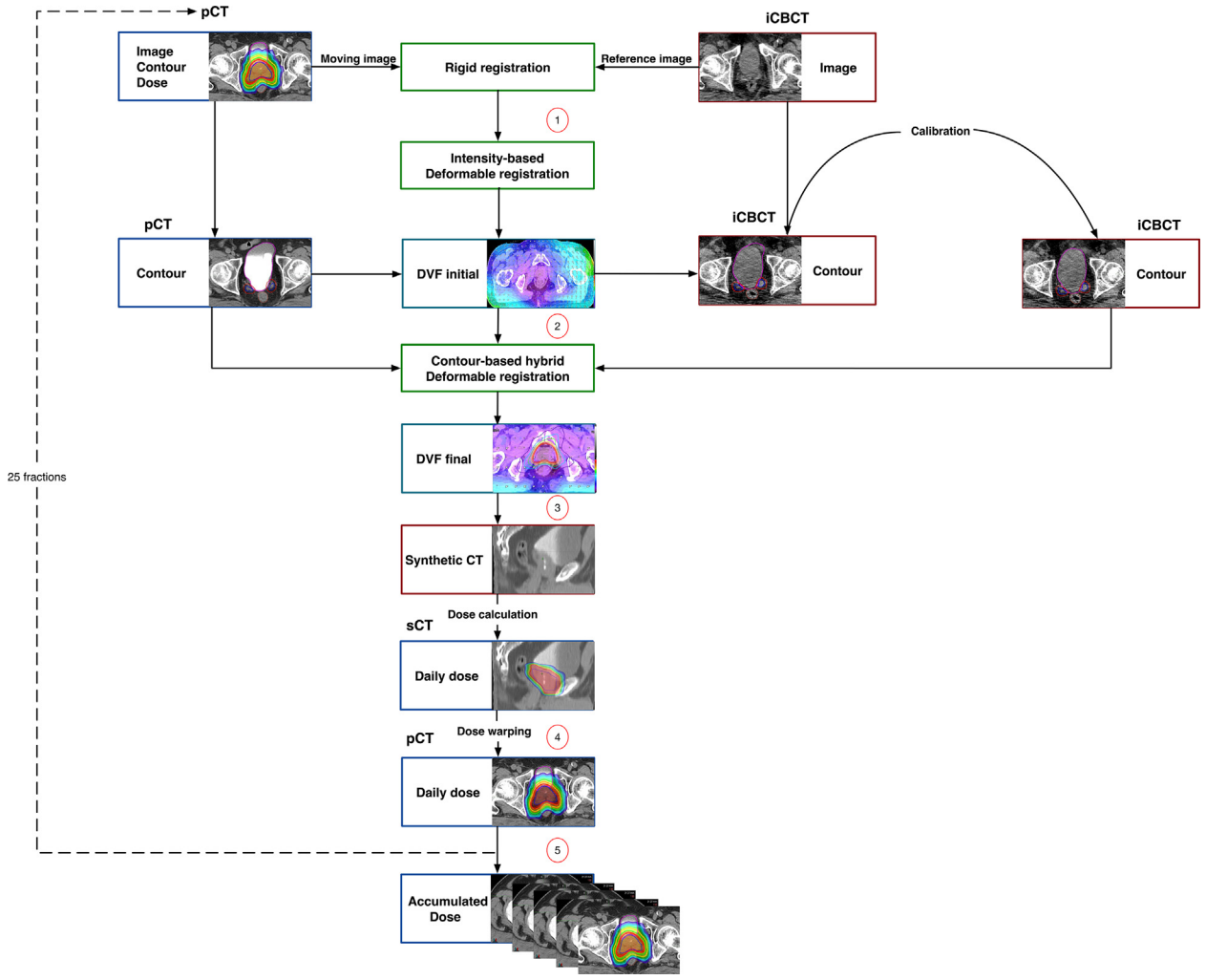

Figure 1 Dose accumulation workflow: (1) The pCT was initially rigidly registered, followed by intensity-based deformable registration onto the daily iCBCT to obtain the initial DVF and contours; (2) the pCT was contour-based hybrid deformably registered onto the daily iCBCT after calibrating rectum and bladder delineations by the same physician, resulting in the final DVF; (3) synthetic CT (sCT) combined the electron density of pCT with the contour structure of iCBCT was created and the daily dose was calculated; (4) after that, the daily dose was warped onto the pCT; (5) steps from 1 to 4 were repeated for each of 25 fractions and the accumulated dose was accepted.

Abbreviations: CT = computed tomography; DVF = deformation vector field; iCBCT = iterative cone beam computed tomography; pCT = planning CT; sCT = synthetic CT.

Image registration and contour propagation (Fig. 1 (1), (2))

The planning CT was initially rigidly registered, followed by deformable registration onto the daily iCBCT, which employs a constrained, intensity-based algorithm to minimize voxel HU differences. The initial deformation vector field (DVF) and contours were obtained from the planned CT to the fraction CT. Maintaining consistent bladder volume was challenging despite educating patients on rectal emptying and bladder-filling protocols. To address bladder volume changes, the same physician adjusted the CTV, bladder, and rectum contours on CBCT, followed by contour-based hybrid DIR.

sCT generation and dose calculation (Fig. 1 (3))

The final DVF was used to deform pCT into CBCT, creating a synthetic CT that preserved the CT's electron density and CBCT's structure. Dose calculations were performed in the Eclipse system after adjusting couch shifts and scaling the fractional dose. The CT image origin was set by the isocenter coordinates of skin markers in the simulation room, while the actual sCT isocenter was determined from each patient's treatment couch shift data.

Dose accumulation (Fig. 1 (4)(5))

The sCT daily doses were converted to the pCT using the final DVF and repeated 25 times. These doses were

then combined on the pCT to calculate the patient's final accumulated dose.

DIR validation

DIR is influenced by algorithms and parameters, leading to multiple solutions. Uncertainty is notable in sliding and uniform regions, necessitating quantification of uncertainty in dose accumulation. This includes geometric indicators like dice similarity coefficient (DSC) and mean distance to agreement (MDA), DVF's physical property index such as the Jacobian determinant, and voxel position and dosimetric indicators like the distance discordance metric (DDM) value and δ index.

Geometrical verification

To evaluate the concordance between radiation oncologist's and DIR propagated contours, the DSC[23] and MDA[24] were calculated. They were used to quantify the degree of volume overlap and the mean 3-dimensional distances between 2 contours, respectively. A DSC value of $\geq$0.8 and MDA of <3 mm are deemed acceptable.[24]

Physical properties of DVF

The Jacobian determinant (J) was computed for each voxel to evaluate local deformation in the DVF.[25] J values indicate local volume changes: $J > 1$ for expansion, $J < 1$ for compression, and $J = 1$ for no change. Voxels with $J < 0$, suggesting implausible deformations, were examined for their proportion and distribution to ensure the DIR results' consistency and biomechanical validity. To evaluate physiological plausibility, Jacobian determinant statistics (mean $\pm$ SD) and the proportion of voxels within predefined Jacobian range were calculated for each structure: CTV ($0.8 \leq J \leq 1.2$), rectum and bladder ($0.6 \leq J \leq 1.4$). Voxels outside these ranges were flagged as potentially unreliable for further voxel-level dose analysis.

Voxel position and dosimetry uncertainty

Spatial uncertainty was quantified using the DDM,[26] which calculates the SD of a voxel's end-position after completing a full cycle through all fractional DVFs. A higher DDM indicates greater registration uncertainty. The average DDM values for the rectum, bladder, and CTV were reported.

Dosimetric uncertainty

The δ index measures dose accumulation uncertainty by assessing potential dose deviations within a voxel's neighborhood, defined by its DDM.[26] It identifies any voxel with a dose difference exceeding 2% from the reference voxel, accounting for spatial uncertainty and local dose gradients. A δ index above 1 suggests unreliable dose accumulation. The δ index passing rate (percentage of voxels with δ index $\leq$1) was calculated for clinical evaluation, reflecting the reliability of the accumulated dose distribution at specific levels. Passing rates were assessed for the whole body at 80% and 40% of the prescription dose (PD80% and PD40%).

Nondeformable DVH summation

A nondeformable DVH summation, referred to as Rigid_SUM, was utilized as a reproducible benchmark to validate the dose accumulation based on DIR. Daily doses were recalculated on sCTs, and dose–volume parameters were aggregated across fractions without employing deformable registration. This method offers a mathematically consistent and registration-independent evaluation of cumulative dose, providing a robust reference for assessing the accuracy of the DIR approach.

Margin verification and dosimetry assessment

The accumulative dose delivered to CTV/DIL, rectum, bladder, and urethra was calculated and compared with the planned dose to verify the feasibility of the margin. Then, the dose was converted to the equivalent dose in 2 Gy fractions (EQD2) based on the linear-quadratic model.

To account for all volume-dose parameters, the tumor's generalized equivalent uniform dose was calculated with an a-value of -4 as biological indicators.[27] Furthermore, clinical outcomes were compared by using Lyman-Kutcher-Burman NTCP model with $n = 0.02$, $m = 0.07$, and TD50 = 77.9 Gy for grade >2 GI toxicity, and similarly $NTCP_{bladder}$ with $n = 0.12$, $m = 0.24$, and TD50 = 81.7 Gy for grade >2 GU toxicity.[28]

$$NTCP = \frac{1}{\sqrt{2\pi}} \int_{-\infty}^{t} e^{-\frac{x^2}{2}} dx \tag{4}$$

$$t = \frac{EUD - TD_{50}}{mTD_{50}} \tag{5}$$

$$EUD = \left(\sum_i v_i D_i^{\frac{1}{n}} \right)^n \tag{6}$$

TD_{50} is the dose causing adverse reactions in 50% of tissues; EUD is the equivalent uniform dose; Parameters m and n indicate the dose-response curve slope and volume dependence.

Furthermore, the dosimetric indicators and toxicity results verified the variations in different matching methods (Fig. E2). There are 2 groups: (1) rectal anterior wall-based matching: daily CBCT scans were adjusted using initial bone-matching, then prostate-matching, with important adjustments based on the rectum's anterior wall. (2) prostate-based matching: Daily CBCT scans were adjusted just prostate-based matching. The

accumulative doses (Da) from the 2 matching methods were Da_Rectum and Da_Prostate.

Statistics

The differences in rectal and bladder volume were compared with the 2-tailed paired *t*-test using SPSS Software (version 26). The delivered and planned physical and biological indices were compared using paired *t* tests if they were normally distributed, using the Wilcoxon rank test. Correlation of geometric measurement, volume change, and dosimetry parameters between 2 groups of studied parameters, planned and actual dose volume, was analyzed by Spearman's rank correlations (r_s). Logistic regression was employed to examine the factors associated with DIL deficit, build a multivariate model, and identify the cut-off value. Statistical significance was set at $P < .05$.

Results

Evaluation of deformation effects

Deformable rationality

The deformation registration of CT images to iCBCT images, as illustrated in Figure E3, demonstrates that the iCBCT field of view is adequately extensive, with high soft-tissue resolution. Compared to intensity-based DIR, contour-based DIR produces more realistic deformations, especially for bladders with significant volume changes, while maintaining the shape of pelvic bones and avoiding peripheral image distortion. This is supported by an organ-wise Jacobian analysis, showing an absence of nonphysical deformations ($J < 0$) across all structures. The majority of voxels underwent deformations within plausible ranges: 92.23% for CTV, 89.63% for rectum, and 88.96% for bladder (Table E1). Jacobian mapping (Fig. E4) further indicated that voxels outside the plausible ranges were mainly located in the bladder dome and rectosigmoid flexure, away from high-dose areas adjacent to the targets.

Geometrical verification

Figure 3 shows changes in bladder and rectal volumes during treatment compared to pCT. The mean bladder CBCT volume was significantly smaller than pCT (319.92 $cm^3 \pm 134.28$ cm^3 vs 364.05 $cm^3 \pm 105.62$ cm^3, $P < .01$) and had a strong correlation with daily calculation dose of V40-60 (rs = 0.72, $P < .01$) in sCT, but a weak correlation with D1cc of CTV and Dmean of the trigone (rs = −0.32, $P < .01$). The rectal volume slightly increased (61.48 $cm^3 \pm 23.25$ cm^3 vs 64.58 $cm^3 \pm 24.33$ cm^3, $P < .01$) and showed a weak correlation with V70 Gy of CTV (rs = −0.288, $P < .01$) and Dmean of the trigone (rs = 0.332, $P < .01$). The findings showed that bladder volume influenced self-dose and high dose in the target and trigone, while rectal volume impacted target coverage and average dose in the trigone, with coefficients of variation at 0.42 and 0.37, respectively. Typically, bladder volume management is stringent, treating only patients with bladder filling within ±30%; others must pause treatment and refill their bladder. Results obtained from geometrical analysis comparison between the final propagated and manual contours are as follows: CTV (DSC: 0.89 ± 0.01, MDA: 0.26 ± 0.04 mm), rectum (DSC: 0.95 ± 0.04, MDA: 0.43 ± 0.42 mm), and bladder (DSC: 0.93 ± 0.10, MDA: 0.89 ± 0.68 mm) were within clinically accepted tolerances for both DSC (>0.8) and MDA (<3 mm).

Spatial and dosimetric uncertainty

The mean DDM values ranged from 0.01 mm to 10.25 mm for the whole body, 1.37 to 3.86 mm for CTV, 2.16 to 6.05 mm for rectum, and 2.23 to 7.33 mm for bladder. Figure 4 illustrates the voxel-wise distributions of DDM, accumulated dose, and δ index passing rate (PD40%) for 5 representative patients. Over 95% of CTV and rectum voxels had DDM <3 mm, and over 90% of bladder voxels had DDM <5 mm, with larger values at the skin surface and bladder dome. δ index passing rates ranged from 77.70% to 92.32% at PD40% and 82.09% to 93.10% at PD80% (mean ± SD: 90.04% ± 5.92). Voxels failing the δ criterion were mainly in areas with steep dose gradients, like the bladder base, prostate apex, and CTV near the anterior rectal wall.

Comparison with Rigid_SUM

Systematic differences were observed between the DIR-based accumulated dose (Da_Rectum) and the nondeformable benchmark (Rigid_SUM). DIR achieved better target coverage with higher PTV D95% (66.39 Gy vs 65.12 Gy, $P < .05$) and CTV V95% (98.40% vs 97.53%, $P < .05$) (Table 1). For rectal protection, DIR significantly reduced high-dose exposure, especially in V65 (0.11% vs 0.98%, $P < .05$). A similar trend was observed in the bladder, with a lower high-dose volume (V73.5cc: 5.23 cm^3 vs 6.43 cm^3, $P < .05$). These findings indicate that DIR offers a more accurate dose representation by considering organ motion and deformation.

Comparison of planned dose and delivered dose

Compared to the planned dose (Dp), the Da of PTV using daily soft-tissue matching statistically decreased, with the median D95% dose dropping from 70.08 Gy to 66.39 Gy. Da of D95%_CTV dropping from 70.98 Gy to 69.98 Gy, with slightly decreased, and 65 Gy coverage remained adequate (Table 1). Patients had 1 to 2 DIL

Table 1 Comparison of planned versus delivered doses for target volumes and organs at risk across various matching strategies

	ROI	Dp	Da_Rectum	Da_Prostate	Rigid_SUM
PTV					
	D95% (Gy)	70.08 (69.45-70.51)	66.39 (64.18-67.79) *	66.41 (63.17-67.61)	65.12 (63.03-66.66) †
	V65Gy (%)	99.22 (98.71-99.62)	96.70 (94.13-97.12) *	96.69 (93.91-98.68)	94.96 (93.60-96.27) †
	V70 (%)	95.19 (93.82-96.23)	86.00 (83.92-89.93) *	85.88 (82.41-89.89)	86.89 (84.29-88.53)
CTV					
	D2% (Gy)	76.04 ± 0.68	75.81 ± 0.78	75.53 ± 0.76 ‡	75.65 ± 1.02 †
	D98% (Gy)	69.27 (68.17-70.20)	67.14 (64.78-68.25) *	67.31 (65.17-69.32)	66.12 (63.58-67.27) †
	D95% (Gy)	70.98 (70.62-71.53)	69.98 (68.38-70.85) *	69.75 (68.07-71.33)	69.49 (67.66-70.21) †
	V95% (%)	99.41 (99.08-99.75)	98.40 (96.79-98.99) *	98.49 (96.89-99.74)	97.53 (96.14-98.33) †
	V65Gy (%)	100.00 (99.99-100.00)	99.13 (98.84-99.54) *	99.28 (99.85-99.92)	98.39 (97.22-98.90) †
	V70 (%)	97.34 (96.26-98.20)	94.97 (92.65-96.15) *	93.92 (90.92-97.26)	94.13 (93.30-95.61)
DIL					
	D99% (Gy)	71.63 (70.22-72.57)	71.93 (68.67-72.81)	72.15 (68.65-73.04)	71.68 (66.29-72.18) †
	D100% (Gy)	70.53 (69.13-72.16)	71.51 (68.71-72.59)	71.45 (67.82-72.54)	71.00 (65.00-71.89) †
	Dmean (Gy)	74.24 (73.79-74.52)	74.64 (74.05-75.03)	74.41 (73.37-74.74)	74.52 (73.91-74.86)
Rectum					
	D0.03cc (Gy)	64.49 ± 1.59	65.71 ± 2.51*	67.04 ± 2.51	68.49 ± 2.08 †
	V65 (%)	0.03 (0.00-0.07)	0.11 (0.03-0.68) *	0.34 (0.15-1.57)	0.98 (0.67-1.54) †
	V62.5 (%)	0.51 (0.23-0.84)	0.53 (0.37-1.60)	1.52 (0.48-3.45) ‡	1.83 (1.32-2.81) †
	V60 (%)	1.78 (1.40-2.29)	1.35 (1.06-2.83)	3.21 (0.99-5.60) ‡	3.08 (2.18-4.59) †
	V50 (%)	9.76 (8.05-10.78)	7.91 (6.83-14.17)	14.14 (7.98-17.35) ‡	9.16 (7.92-13.06)
	V40 (%)	20.89 (18.41-24.08)	20.41 (17.67-29.89)	24.02 (20.36-30.42) ‡	19.89 (17.90-30.35)
	Dmean (Gy)	25.20 ± 4.57	25.80 ± 5.35	26.81 ± 5.66 ‡	26.09 ± 4.77
Bladder					
	V73.5 (cm3)	4.32 (1.20-6.38)	5.23 (1.42-7.36)	1.21 (0.18-2.20) ‡	6.43 (3.51-8.91) †
	V70 (cm3)	10.33 (8.22-15.72)	11.16 (7.14-16.64)	7.80 (4.81-9.75) ‡	14.80 (8.33-19.80) †
	V60 (%)	5.61 (4.03-8.30)	7.20 (4.83-10.38) *	5.91 (4.42-7.83) ‡	7.40 (4.70-10.18)
	V50 (%)	9.92 (6.03-13.07)	10.96 (7.61-16.37) *	10.33 (6.80-12.91) ‡	10.97 (7.00-16.08)
	V40 (%)	15.74 ± 7.18	18.31 ± 7.57 *	16.82 ± 6.48 ‡	18.72 ± 7.58
	Dmean (Gy)	17.72 ± 6.98	20.16 ± 7.54 *	19.22 ± 6.89 ‡	21.32 ± 7.13
Wall					
	D0.03cc (Gy)	76.00 ± 1.27	75.31 ± 0.86 *	74.46 ± 0.91 ‡	76.31 ± 0.68 †
	V73.5 (cm3)	3.96 (1.19-5.24)	4.35 (1.38-5.91)	1.21 (0.18-2.20) ‡	3.91 (2.89-6.47) †
	V60 (%)	11.98 ± 4.67	11.75 ± 3.76 *	10.60 ± 2.99 ‡	13.66 ± 4.25 †
	Dmean (Gy)	20.03 ± 5.94	21.28 ± 6.03 *	20.48 ± 5.48 ‡	22.15 ± 4.80
Trigone					
	D0.03cc (Gy)	75.45 (73.92-76.13)	74.68 (73.45-75.17)	73.16 (70.76-74.48) ‡	75.83 (74.63-76.41) †
	V73.5 (cm3)	0.70 (0.19-1.63)	0.22 (0.02-1.80)	0.01 (0.00-0.42) ‡	0.85 (0.53-2.61) †
Urethra					
	D0.03cc (Gy)	75.59 ± 0.98	75.56 ± 0.86	75.14 ± 0.90 ‡	76.07 ± 0.89 †
	V73.5 (cm3)	1.28 (0.89-2.56)	1.83 (0.98-2.41) *	1.38 (0.71-2.45) ‡	1.74 (0.96-2.52)

Abbreviations: CTV = clinical target volume; Da_Prostate = accumulative dose based on prostate matching; Da_Rectum = accumulative dose based on anterior rectal wall matching; DIL= dominant intraprostatic lesion; Dp = planned dose; PTV = planned target volume; Rigid_SUM = nondeformable dose summation.

Statistical significance was assessed using matched-pairs t-tests for normally distributed data, and Wilcoxon signed rank tests for non-normal data. */†/‡Indicate significant differences. Customarily distributed values are presented as mean ± SD, while non-normal distributions are shown as medians with quartiles.

Table 2 An overview of the 23 patients' dominant intraprostatic lesion (DIL)

Patient	DIL			
	Volume	Location	Direction	Number
1	4.50	mid (TZp+PZpm)	post	1
2	4.90	base+mid (AFS+TZa/p)	ant	1
3	1.30	mid (PZpm)	post	1
4	15.90	mid(TZa)	ant	1
5	4.60	mid+apex (PZpl)	post	1
6	3.29	mid (AFS)	ant	2
	1.29	mid (PZpm)	post	
7	3.70	mid (PZpl)	post	1
8	2.40	base (PZpl)	post	1
9	1.78	mid (PZpm)	post	1
10	1.52	apex (TZpl+PZpm)	post	2
	0.92	apex (TZa+PZa)	ant	
11	5.94	base (AFS+TZa)	ant	1
12	6.45	mid (TZa)	ant	1
13	9.85	mid (TZa)	ant	1
14	5.24	base (AFS+TZa)	ant	1
15	10.31	base (AFS+TZa)	ant	1
16	5.67	mid (PZpm)	post	1
17	0.55	mid (TZa)	ant	1
18	9.43	mid (TZa+PZa)	ant	1
19	13.72	mid (TZa/p+PZpm/pl)	post	1
20	1.42	base (TZa)	ant	1
21	4.55	mid+apex (TZa+AFS)	ant	2
	0.79	mid (PZpm)	post	
22	2.32	Bace (AFS+TZa)	ant	1
23	1.54	mid+apex (Tzp+PZpm)	post	1

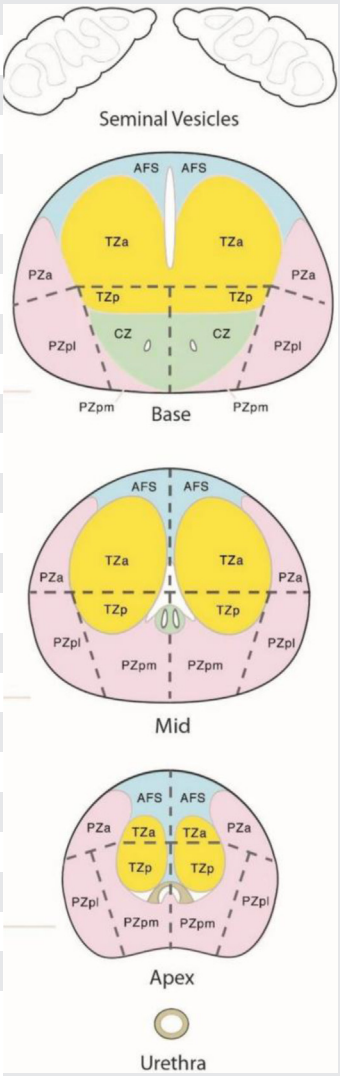

Abbreviations: AFS = anterior fibromuscular stroma; ant = anterior; post = posterior; PZ = peripheral zone; TZ = transition zone.
Sector map of the prostate, modified after Weinreb et al.[33]

lesions, with 42.1% in the transition zone, 39.5% in the peripheral zone, 18.4% in the anterior fibromuscular stroma, and with a median volume of 3.70 cm^3 (1.47-6.19 cm^3) (Table 2 and Fig. E5). The median D100% dose for DILs increased from 70.53 Gy to 71.51 Gy, maintaining target coverage. However, in 3 patients, the prescribed dose was inadequate due to the DILs' proximity to the rectum's anterior wall. Univariate analysis revealed significant correlations between the minimum distance (d_{min}) from the anterior rectal wall to the DIL (OR = 0.25, P = .008) and the rectal volume overlapping with DIL_{2cm} (V_{DIL2}) (OR=1.42, P = .032) with the actual DIL deficit. The optimal cut-offs were 0.7 mm for d_{min} (AUC=0.88, sensitivity 85%, specificity 80%) and 1.5 cm^3 for V_{DIL2} (AUC = 0.76, sensitivity 75%, specificity 70%). Clinically, if d_{min} is less than 0.7 mm and V_{DIL2} exceeds 1.5 cm^3, there is a heightened risk of insufficient DIL dose, suggesting a need to adjust the target expansion range. The V40 Gy-V60 Gy of the bladder increased significantly. Aside from a minor increase in D0.03cc and V65 Gy for the rectum's high-dose area, other dose-volume parameters remained stable.

In contrast to prostate-based matching, evidence indicates soft-tissue matching based on the anterior rectal wall offers better target coverage and rectal protection. Still, caution is needed regarding increased high-dose

Table 3 Comparison of biological indicators for target volumes and organs at risk across different matching strategies

	Dp	Da_Rectum	Da_Prostate
EUD prostate (Gy)	99.34 ± 3.49	97.45 ± 3.68*	96.95 ± 3.42
ΔEUD prostate (Gy)	–	−1.78 (−2.31 to −0.31)	−1.83 (−2.16 to −1.21)
NTCP rectum (%)	9.08 (6.96 to 13.62)	7.95 (4.13 to 13.51)	13.61 (3.31 to 19.11‡)†
ΔNTCP rectum (%)	–	−3.71 (−4.95 to 2.39)	3.24 (−2.33 to 12.31)
NTCP bladder (%)	15.64 (12.34 to 20.79)	16.39 (11.93 to 20.19)*	15.28 (11.05 to 19.04‡)†
ΔNTCP bladder (%)	-	−0.15 (−1.52 to 1.04)	−2.01 (−2.40 to 0.13)

Abbreviations: Da_Prostate = accumulative dose based on prostate matching; Da_Rectum = accumulative dose based on anterior rectal wall matching; Dp = planned dose; EUD = equivalent uniform dose; NTCP = normal tissue complication probability.
Statistical significance was assessed using matched-pairs *t* tests for normally distributed data, and Wilcoxon signed-rank tests for non-normal data.
*,†Indicate significant differences. Normally distributed data are shown as mean ± SD, non-normal data as medians with quartiles.

exposure in the bladder trigone and urethra. Further analysis of dose distribution revealed that insufficient CTV target coverage was primarily located in the rectal anterior wall, while the delivered dose to the prostate apex was adequate.

Comparison of toxicity results

In contrast to prostate-based matching, soft-tissue matching based on the anterior rectal wall offers better target coverage and rectal protection. The trends observed in biological indicators generally align with those of physical parameters. The mean EUD delivered to the target demonstrated a statistically significant reduction of 1.89 Gy. Bladder NTCP remained consistent with the planned values. In comparison to simple prostate-based alignment, fine-tuning the anterior rectal wall provides better rectal protection (NTCP 7.95% vs 13.61%) while maintaining target coverage (EUD 97.45 Gy vs. 96.95 Gy) (Table 3).

Discussion

Interfractional organ motion and deformation introduce uncertainties in prostate and OAR dose delivery, impacting tumor control and toxicity risks.[29] This study observed significant prostate displacements and volume variations despite rigorous rectal/bladder preparation. Hypofractionation exacerbates these challenges due to steep dose gradients, necessitating institution-specific CTV-PTV margins.

A customized workflow was developed to incorporate daily organ volume variations for cumulative dose calculation to the prostate and OARs (Fig. 2). The daily dose was calculated using sCT for accurate electron density representation. DIR was used to transfer these doses back to pCT for summation, ensuring spatial consistency and reliable local dose accumulation for accurate DVHs.[30] To quantify uncertainties associated with the hybrid contour-based DIR,[19-21,31] a multilevel validation was conducted. Beyond standard geometric metrics—DSC > 0.8 and MDA < 3 mm—a biomechanical assessment based on the Jacobian determinant (J) was conducted. This analysis revealed that over 88% of voxels within critical structures experienced deformations within expected ranges. Specifically, the CTV exhibited high stability, the rectum showed mild volumetric changes, and the bladder demonstrated a wide spectrum of Jacobian values, consistent with its variable filling status. The fact that the majority of voxels in relevant structures displayed J-values between 0.5 and 1.5 supports the biomechanical plausibility of the DIR-predicted deformations, particularly in regions adjacent to treatment targets, thereby validating the use of DIR for dose accumulation in these areas. Spatial uncertainty, measured by the DDM, was low in key structures, confirming registration robustness. The δ index provided voxel-wise dose confidence, highlighting higher uncertainties in high-gradient areas, with overall passing rates between 77.7% and 93.1% at PD40%-PD80% dose levels. This approach boosts confidence in dose accumulation accuracy and underscores the δ index's clinical importance for identifying significant dose uncertainties.

Moreover, a comparison with a nondeformable DVH summation benchmark demonstrated that DIR-based accumulation provided superior target coverage and a reduction in high-dose volumes to OARs. This distinction arises from DIR's capability to account for voxel-level tissue motion, thereby generating a more physiologically accurate dose accumulation model. In this model, high-dose regions are distributed over a larger volume due to organ deformation, rather than being rigidly superimposed. As a result, nondeformable methods may underestimate therapeutic efficacy while overestimating toxicity risks, underscoring the clinical value of DIR for precise dose assessment.

A 5-mm CTV-to-PTV margin with posterior rectal trimming was used to deliver 70 Gy/25 f (EQD_2 = 81.2 Gy, α/β = 3), focusing on rectal protection with constraints of D_{max} < 70 Gy and V65 < 0.01%. Compared to the CHHiP protocol (60 Gy/20 f, EQD_2 = 72 Gy, α/β=3),[7] our approach offered a higher biological dose. Potter et al[32]

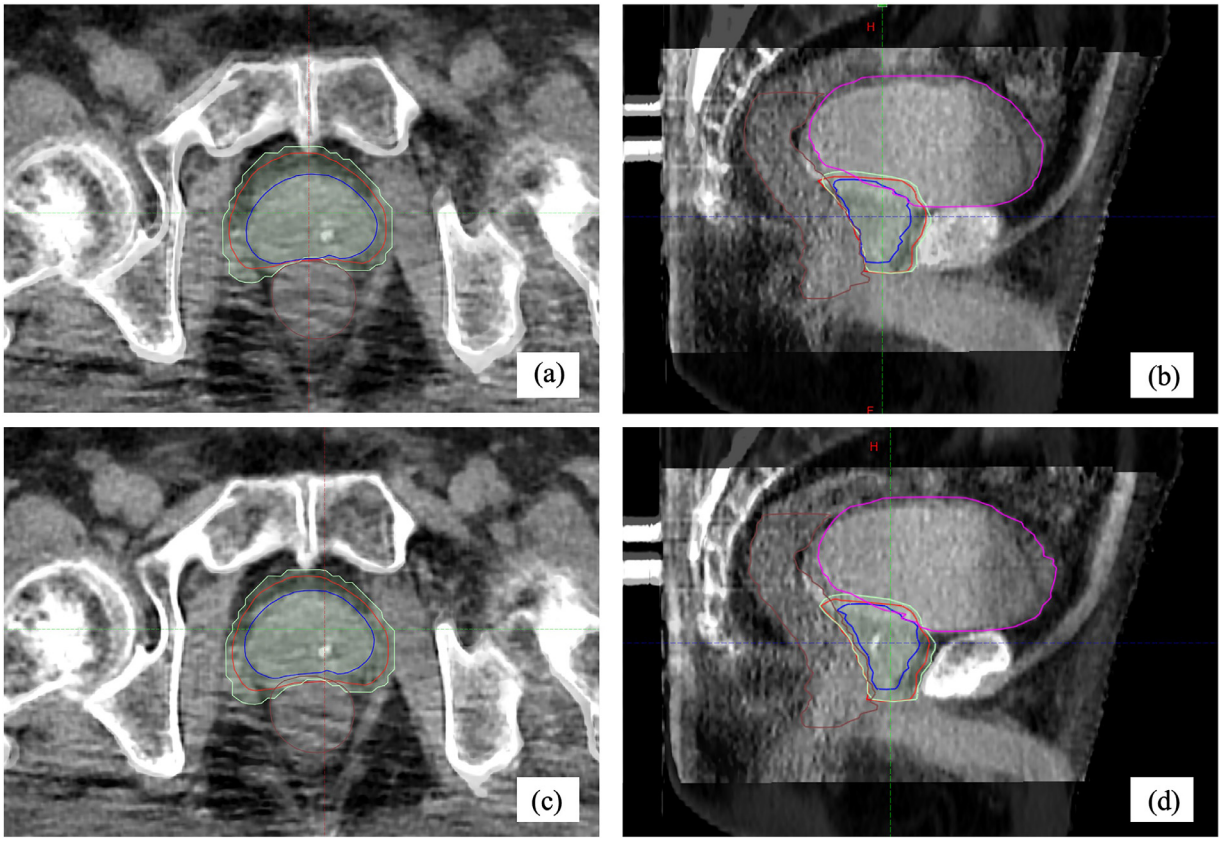

Figure 2 Axial and sagittal view of CBCT 11 patient 8 based on soft tissue (a,b) and prostate-based matching methods (c,d). On the planning CT, the PTV is shown by the red line and the 65 Gy dose by the green translucent line, while the CBCT displays the bladder in purple, the rectum in brown, and the CTV in blue.
Abbreviations: CBCT = cone beam computed tomography; CT = computed tomography; CTV = clinical target volume; PTV = planning target volume.

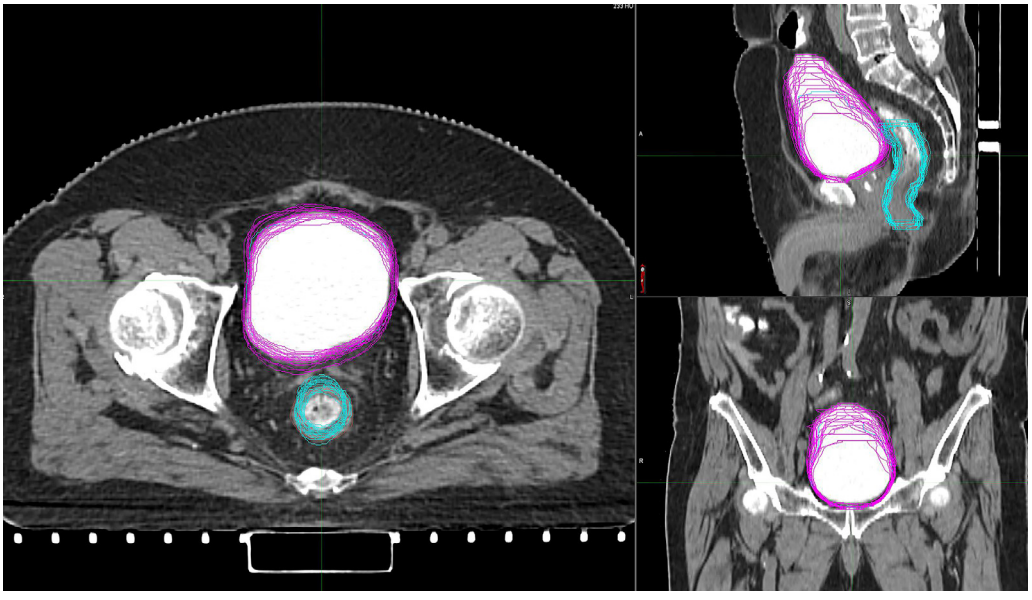

Figure 3 Schematic diagram of bladder and rectal volume changes. The purple lines represent the bladder volumes and green lines represent the rectal volumes at different treatment fractions.

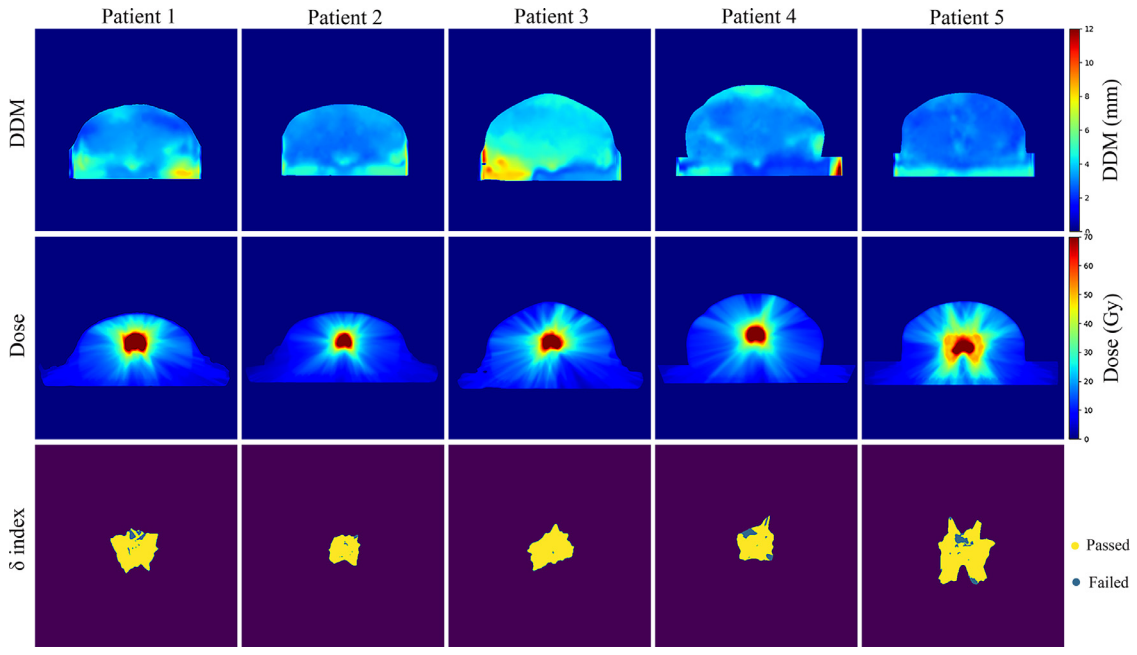

Figure 4 The distance discordance metric (DDM), accumulated dose and voxels failing or passing the δ index criteria for threshold dose of 40% of the prescription dose (PD40%) for 5 patients.

found that keeping the rectal D2cc $\leq$ 65 Gy reduces radiation enteritis risk by 10%. With D2cc doses between 60 and 65 Gy, 8.6% of patients experienced grade $\geq$2 rectal side effects over 3 years. For targets near the anterior rectal wall, a dose of 65 Gy (EQD2 = 72.8 Gy, α/β = 3) is deemed sufficient (Fig. E1). Image guidance utilized a novel 65 Gy isodose line (Dose_65Gy) as the anterior rectal wall reference. This 3-step alignment protocol (bone-prostate-rectal anterior wall) achieved comparable target coverage with reduced grade $\geq$2 GI toxicity (7.95% vs 13.61%) versus prostate-based alignment. Dose_65Gy optimization minimized interobserver variability at the critical prostate-rectum interface. This was consistent with Zhang et al,[18] which showed that interobserver variability is mainly in the anterior rectal wall, not the prostate.

DIL coverage is influenced by its proximity to the anterior rectal wall. Combining PSMA-PET/CT and mpMRI improves DIL delineation, revealing their primary distribution in the transitional and peripheral zones. Assuming DILs are stable within the prostate, with no additional boost dose applied, a full 70 Gy dose is required for complete coverage, though 65 Gy suffices for CTV. In 3 cases, DILs near the anterior rectal wall and unclear CBCT boundaries led to dose reduction, highlighting the importance of DIL location. DIL deficit risk increases when the anterior rectal wall is less than 0.7 mm from the DIL and a 2 cm rectal extension overlaps more than 1.5 cm^3 with the DIL. A 2 to 3 mm margin is advised,[33] prioritizing image matching on the prostate area with DIL, then adjusting for the anterior rectal wall, despite potential rectal toxicity. Using spacerOAR (hydrogel) between the rectum and prostate may be preferable.

Dose accumulation revealed effective rectal protection (NTCP = 7.95%) but increased bladder V40 Gy-V60 Gy due to treatment-related volume reduction. Paradoxically, trigone V70 Gy~V73.5 Gy, 16/23 patients decreased. This may be due to the bottom end of the trigone being fixed at the urethral opening, and there was often an anterior and inferior displacement during treatment. Despite only 2% volume of the bladder, the trigone showed significant movement and deformation.[34] For grade $\geq$2 GU toxicity, the median NTCP for the bladder was 16.39%. In the real world, 382 patients with limited-stage prostate cancer (T1-4N0M0) received radical radiation therapy and were assessed for toxicity using a modified RTOG standard between 2016 and 2020. Advanced GU toxicity (grade $\geq$2) occurred in 19.9% of cases, with symptoms like frequent urination, urinary incontinence, difficulty urinating, and hematuria. Advanced GI toxicity (grade $\geq$2) was seen in 11.1% of cases, with symptoms such as bloody stool, increased defecation frequency, and fecal incontinence. Real-world rectal and bladder toxicity rates were higher than calculated rates, likely due to differences in classification, data bias, and follow-up duration. This study highlights comparative differences, allowing for the disregard of these biases.

To reduce the CTV-PTV margin effectively, a thorough assessment of the treatment process is crucial. This includes precise delineation of DIL, CTV, and OAR, strict rectal and bladder preparation, a stable treatment plan, daily image guidance, advanced radiation therapy

technologies, and shorter treatment durations. A previous study used the Clarity ultrasound system for real-time monitoring of prostate motion, showing displacements within 1 mm in 83.07%, 85.46%, and 78.27% of measurements along the x, y, and z axes, respectively.[35] In the current study, treatment with a Halcyon ring gantry linac had an average beam-on time of 1.97 minutes per fraction, making intrafraction motion negligible. However, in 20.53% of fractions, the CTV_V95% objective of 98% was not met, indicating that a zero margin toward the anterior rectal wall requires careful evaluation.

This study is pioneering in its proposal of precise anterior rectal wall matching and employs daily iCBCT along with contour-based mixed DIR to assess the cumulative dose and toxicity affecting the DIL and rectum. However, it did not account for uncertainties related to prostate rotation, intrafraction movement, contouring, and accelerator precision. Additionally, the study's sample size was limited, and there was an absence of correlation analysis between toxicity and cumulative dosimetric parameters. Ongoing work applies this workflow to larger cohorts to develop predictive models for tumor control and toxicity. Future integration of intrafraction monitoring and AI-driven adaptive strategies could further optimize therapeutic ratios.

Disclosures

None.

Acknowledgments

The authors express sincere gratitude to Dr. Xuesong Li from the Department of Urology for his invaluable clinical guidance and critical insights throughout this study. We also acknowledge the radiation therapy team for their precise implementation of the image-guidance protocol. Special thanks to Dr. Bo Zhao (National Institutes for Quantum Science and Technology, Japan) for his expertise in deformable image registration methodologies. We deeply appreciate all participating patients for their cooperation and commitment. Gao Yan and Huang Lei are responsible for statistical analysis.

Supplementary materials

Supplementary material associated with this article can be found in the online version at doi:10.1016/j.prro.2025.10.020.

References

1. Faccenda V, Panizza D, Daniotti MC, et al. Dosimetric impact of intrafraction prostate motion and interfraction anatomical changes in dose-escalated linac-based SBRT. *Cancers (Basel)*. 2023;15:1153.
2. Bostel T, Sachpazidis I, Splinter M, et al. Dosimetric impact of interfractional variations in prostate cancer radiotherapy-implications for imaging frequency and treatment adaptation. *Front Oncol*. 2019;9:940.
3. Ong A, Knight K, Panettieri V, et al. Development of an automated radiotherapy dose accumulation workflow for locally advanced high-risk prostate cancer—A technical report. *J Med Radiat Sci*. 2021;68:203-210.
4. Wang G, Wang Z, Guo Y, et al. Evaluation of PTV margins with daily iterative online adaptive radiotherapy for postoperative treatment of endometrial and cervical cancer: a prospective single-arm phase 2 study. *Radiat Oncol*. 2024;19:2.
5. Brennsaeter JA, Dahle TJ, Moi JN, Svanberg IF, Haaland GS, Pilskog S. Reduction of PTV margins for elective pelvic lymph nodes in online adaptive radiotherapy of prostate cancer patients. *Acta Oncol*. 2023;62:1208-1214.
6. Di Franco F, Baudier T, Gassa F, et al. Minimum non-isotropic and asymmetric margins for taking into account intrafraction prostate motion during moderately hypofractionated radiotherapy. *Phys Med*. 2022;96:114-120.
7. Dearnaley D, Syndikus I, Mossop H, et al. Conventional versus hypofractionated high-dose intensity-modulated radiotherapy for prostate cancer: 5-year outcomes of the randomised, non-inferiority, phase 3 CHHiP trial. *Lancet Oncol*. 2016;17:1047-1060.
8. Van As N, Griffin C, Tree A, et al. Phase 3 trial of stereotactic body radiotherapy in localized prostate cancer. *N Engl J Med*. 2024;391:1413-1425.
9. Incrocci L, Wortel RC, Alemayehu WG, et al. Hypofractionated versus conventionally fractionated radiotherapy for patients with localised prostate cancer (HYPRO): Final efficacy results from a randomised, multicentre, open-label, phase 3 trial. *Lancet Oncol*. 2016;17:1061-1069.
10. Lee WR, Dignam JJ, Amin MB, et al. Long-term analysis of NRG oncology RTOG 0415: A randomized phase III noninferiority study comparing two fractionation schedules in patients with low-risk prostate cancer. *J Clin Oncol*. 2024;42:2377-2381.
11. Murray J, Griffin C, Gulliford S, et al. A randomised assessment of image guided radiotherapy within a phase 3 trial of conventional or hypofractionated high dose intensity modulated radiotherapy for prostate cancer. *Radiother Oncol*. 2020;142:62-71.
12. Groen V H, Haustermans K, Pos F J, et al. Patterns of failure following external beam radiotherapy with or without an additional focal boost in the randomized controlled FLAME trial for localized prostate cancer. *Eur Urol*. 2022;82:252-257.
13. Zamboglou C, Spohn SKB, Adebahr S, et al. PSMA-PET/MRI-based focal dose escalation in patients with primary prostate cancer treated with stereotactic body radiation therapy (HypoFocal-SBRT): Study protocol of a randomized, multicentric phase III trial. *Cancers*. 2021;13:5795.
14. Thureau S, Briens A, Decazes P, et al. PET and MRI guided adaptive radiotherapy: Rational, feasibility and benefit. *Cancer Radiother*. 2020;24:635-644.
15. Zamboglou C, Klein CM, Thomann B, et al. The dose distribution in dominant intraprostatic tumour lesions defined by multiparametric MRI and PSMA PET/CT correlates with the outcome in patients treated with primary radiation therapy for prostate cancer. *Radiat Oncol*. 2018;13:65.
16. Salembier C, Villeirs G, De Bari B, et al. ESTRO ACROP consensus guideline on CT- and MRI-based target volume delineation for

primary radiation therapy of localized prostate cancer. *Radiother Oncol*. 2018;127:49-61.
17. Hirose TA, Arimura H, Fukunaga JI, Ohga S, Yoshitake T, Shioyama Y. Observer uncertainties of soft tissue-based patient positioning in IGRT. *J Appl Clin Med Phys*. 2020;21:73-81.
18. Zhang X, Wang X, Li X, et al. Evaluating the impact of possible interobserver variability in CBCT-based soft-tissue matching using TCP/NTCP models for prostate cancer radiotherapy. *Radiat Oncol*. 2022;17:62.
19. Kim J, Kumar S, Liu C, et al. A novel approach for establishing benchmark CBCT/CT deformable image registrations in prostate cancer radiotherapy. *Phys Med Biol*. 2013;58:8077-8097.
20. Kishigami Y, Nakamura M, Okamoto H, et al. Organ-contour-driven auto-matching algorithm in image-guided radiotherapy. *J Appl Clin Med Phys*. 2024;25:e14220.
21. Kubota Y, Okamoto M, Li Y, et al. Evaluation of intensity- and contour-based deformable image registration accuracy in pancreatic cancer patients. *Cancers (Basel)*. 2019;11:1447.
22. Hodapp N. The ICRU Report 83: Prescribing, recording and reporting photon-beam intensity-modulated radiation therapy (IMRT). *Strahlenther Onkol*. 2012;188:97-99. [in German].
23. Wong WK, Leung LH, Kwong DL. Evaluation and optimization of the parameters used in multiple-atlas-based segmentation of prostate cancers in radiation therapy. *Br J Radiol*. 2016;89:20140732.
24. Brock KK, Mutic S, Mcnutt TR, Li H, Kessler ML. Use of image registration and fusion algorithms and techniques in radiotherapy: Report of the AAPM Radiation Therapy Committee Task Group No. 132. *Med Phys*. 2017;44:e43-e76.
25. Bosma LS, Hussein M, Jameson MG, et al. Tools and recommendations for commissioning and quality assurance of deformable image registration in radiotherapy. *Phys Imaging Radiat Oncol*. 2024;32:100647.
26. Van Den Dobbelsteen M, Hackett SL, Bosma LS, van Doormaal RJA, van Asselen B, Fast MF. Quantifying the spatial distribution of the accumulated dose uncertainty using the novel delta index. *Phys Med Biol*. 2024;70:015003.
27. Wu Q, Djajaputra D, Liu HH, Dong L, Mohan R, Wu Y. Dose sculpting with generalized equivalent uniform dose. *Med Phys*. 2005;32:1387-1396.
28. Basu KS, Bahl A, Subramani V, Sharma DN, Rath GK, Julka PK. Normal tissue complication probability: Does simultaneous integrated boost intensity-modulated radiotherapy score over other techniques in treatment of prostate adenocarcinoma. *J Cancer Res Ther*. 2009;5:78-84.
29. Staffurth JN, Haviland JS, Wilkins A, et al. Impact of hypofractionated radiotherapy on patient-reported outcomes in prostate cancer: Results up to 5 yr in the CHHiP trial (CRUK/06/016). *Eur Urol Oncol*. 2021;4:980-992.
30. Nenoff L, Amstutz F, Murr M, et al. Review and recommendations on deformable image registration uncertainties for radiotherapy applications. *Phys Med Biol*. 2023;68:24TR01.
31. Mao W, Liu C, Gardner SJ, et al. How does CBCT reconstruction algorithm impact on deformably mapped targets and accumulated dose distributions? *J Appl Clin Med Phys*. 2021;22:37-48.
32. Potter R, Tanderup K, Kirisits C, et al. The EMBRACE II study: The outcome and prospect of two decades of evolution within the GEC-ESTRO GYN working group and the EMBRACE studies. *Clin Transl Radiat Oncol*. 2018;9:48-60.
33. Tamihardja J, Cirsi S, Kessler P, et al. Cone beam CT-based dose accumulation and analysis of delivered dose to the dominant intraprostatic lesion in primary radiotherapy of prostate cancer. *Radiat Oncol*. 2021;16:205.
34. Neilsen BK, Ma TM, Akingbemi WO, et al. Impact of interfractional bladder and trigone displacement and deformation on radiation exposure and subsequent acute genitourinary toxicity: A post hoc analysis of patients treated with magnetic resonance imaging-guided prostate stereotactic body radiation therapy in a phase 3 randomized trial. *Int J Radiat Oncol Biol Phys*. 2024;118:986-997.
35. Gao Y, Zhao B, Gao XS, et al. Quantifying intra-fractional prostate motion trajectory for establishing a new gating strategy: a preliminary study. *J. Radiat. Res. Appl. Sci.*. 2020;13:593-600.